Eur. Phys. J. A **10**, 381–385 (2001)

THE EUROPEAN PHYSICAL JOURNAL A

Isospin dependence of the isotopic distributions from ^{36}Ar and ^{40}Ar fragmentation at about 60 MeV/nucleon

D.Q. Fang[1,a], W.Q. Shen[1,3], J. Feng[1], X.Z. Cai[1], Y.G. Ma[1], H.Y. Zhang[1], P.Y. Hu[1], W.L. Zhan[2], Z.Y. Guo[2], G.Q. Xiao[2], J.X. Li[2], M. Wang[2], J.F. Wang[2], Z.J. Ning[2], J.Q. Wang[2], J.S. Wang[2], Q.J. Wang[2], and Z.Q. Chen[2]

[1] Shanghai Institute of Nuclear Research, Chinese Academy of Sciences, Shanghai 201800, China
[2] Institute of Modern Physics, Chinese Academy of Sciences, Lanzhou 730000, China
[3] Ningbo University, Ningbo 315211, China

Received: 15 November 2000 / Revised version: 4 April 2001
Communicated by W.F. Henning

Abstract. Fragments produced in the reactions of 69 MeV/nucleon ^{36}Ar and 55 MeV/nucleon ^{40}Ar on a Be target have been measured experimentally. The isotopic distributions from fragmentation reaction for both projectiles are compared with modified statistical abrasion-ablation model calculations. A strong isospin effect exhibits in the fragment distributions produced in ^{36}Ar and ^{40}Ar fragmentation. Experimental evidence for the disappearance of the isospin effect in the isotopic distributions produced by projectile fragmentation is observed with the increase of the violence of nuclear reaction.

PACS. 25.70.Mn Projectile and target fragmentation – 24.10.-i Nuclear-reaction models and methods

1 Introduction

In the past decades, projectile fragmentation has been widely used to study nuclear reactions induced by heavy ions at intermediate and high energies. Various physical models for projectile or target fragmentation have been developed and the reaction mechanisms of heavy-ion collisions have been investigated extensively [1–7]. Recent advances in experiments using radioactive ion beams (RIBs) with large neutron or proton excess have led to the discovery of neutron skin and neutron halo nuclei such as ^{11}Li, ^{11}Be, etc. [8,9]. Since then, interest in the study of very neutron-rich and proton-rich nuclei has grown in view of their anomalous structures. Projectile fragmentation is one of the most important methods to produce these exotic nuclei and the estimation of the intensity for secondary nuclear beams has become a very important topic. The latest experimental measurement of the production cross-sections for nuclei from stable to the drip-line at relativistic energies has been performed [10]. However, it's difficult for physical fragmentation models to predict the production cross-sections of nuclei far from the β-stability line. Although the empirical parameterization, like EPAX formula presented by Summerer *et al.* [11,12], can predict the fragment production cross-section quite well, the validity of the calculation result depends on the available experimental data. Due to its poor physical foundation, the empirical parameterization may not be applicable in extrapolation. Further experimental and theoretical investigation on the isotopic distributions are expected.

Recently, the isospin effect of various physical phenomena, such as multifragmentation, flow, preequilibrium nucleon emission, etc., have been reported [13–18]. The studies have shown that isospin effect exists in nuclear reactions induced by exotic nuclei but it may disappear under certain conditions. The isospin effect in the production cross-sections from projectile fragmentation has been observed [11,19,20]. The yields of neutron-rich nuclei from fragmentation of neutron-rich projectile will be larger than that from stable nuclei, but the difference becomes smaller with the increase of the charge difference between the fragment and the projectile and disappears at last [19]. This isospin effect and its disappearance can provide not only a valuable insight into the reaction mechanism but also a good reference for producing RIBs. Our work represents an experimental study of the isospin effect of projectile fragmentation by measuring the fragment isotopic distributions from ^{36}Ar and ^{40}Ar fragmentation. A phenomenological investigation of to what extent the obtained yields (after incorporating INTENSITY transmissions) are compatible with modified statistical abrasion-ablation model calculations is performed.

2 Experimental setup

The experiment was performed at the Radioactive Ion Beam Line in Lanzhou (RIBLL) [21] using beams of

[a] e-mail: dqfang@mailcity.com

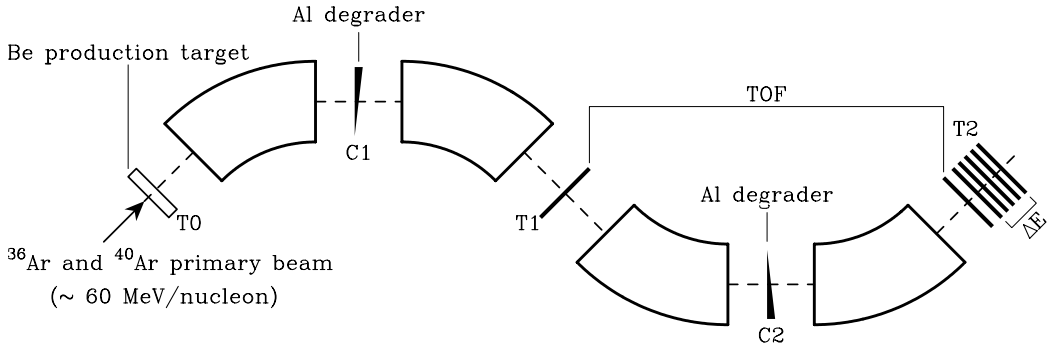

Fig. 1. Experimental setup at RIBLL.

69 MeV/nucleon ^{36}Ar and 55 MeV/nucleon ^{40}Ar which was delivered by the Heavy Ion Research Facility in Lanzhou (HIRFL). A maximum intensity of 60 enA for ^{36}Ar and 40 enA for ^{40}Ar beams was used to produce the fragments. As shown in fig. 1, the Be production target (200 mg/cm^2) was mounted on the target box (T0). After T0, RIBLL can be used as a doubly achromatic magnetic spectrometer where nuclei produced in the reaction were separated and selected by means of magnetic rigidity ($B\rho$) and energy degrader (ΔE). The variable slits and energy degraders, which were made by aluminum foils ($13 \times 10.8\,\mathrm{mg/cm^2}$) and mounted on curved frames, were placed at the dispersive focal plane C1 and C2. The time of flight (TOF) of the fragments was measured by two scintillator detectors installed at the first (T1) and second (T2) achromatic focal planes with a flight path of 16.8 m. A telescope was installed at T2, which consisted of four transmission Si surface barrier detectors followed by a CsI(Tl) crystal and gave the energy losses (ΔE's) and total energy of the reaction products. The thicknesses of the four Si detectors were 150, 150, 700, and 2000 μm, respectively and the energy resolutions were not greater than 0.85%.

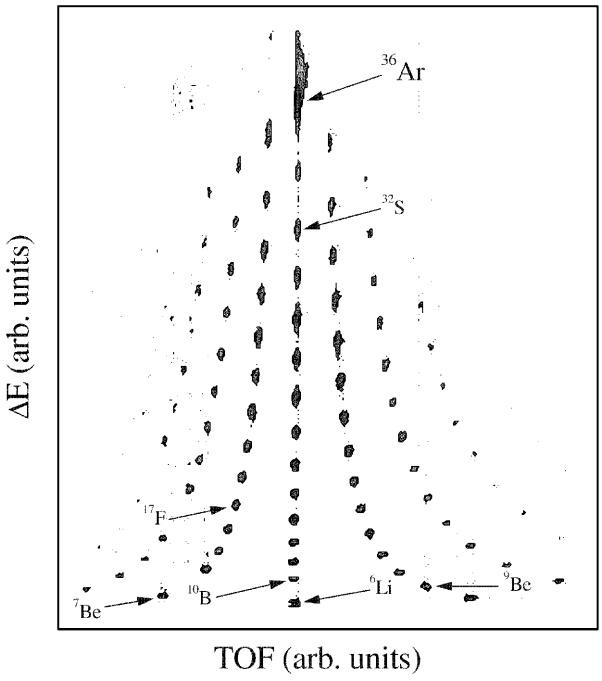

Fig. 2. Two-dimensional contour plot of ΔE *vs.* TOF used as the particle identification for ^{36}Ar.

3 Data analysis and results

After two times of $B\rho - \Delta E - B\rho$ selection of RIBLL, the reaction products can be identified by combining TOF and ΔE in the first Si detector [19,20]. Fragments with $3 \leq Z \leq 17$ were measured and good resolutions were obtained for ^{36}Ar experiment, whereas less fragments were measured for ^{40}Ar experiment because less beam time was used. The fragments from ^{36}Ar and ^{40}Ar fragmentation were measured by a single RIBLL setting, respectively. The particle identification plot for ^{36}Ar is shown in fig. 2. The raw counts obtained with this method are not comparable to theoretical calculations because of the transmission losses for the fragments from T0 to T2. The transmission rate is different for different fragments due to the limited momentum and angle acceptances. The maximum acceptance of RIBLL for momentum and angle was $\Delta P/P \sim 10\%$ and 6.5 msr, respectively. The losses of the fragments in RIBLL were estimated by using the code INTENSITY which is designed to calculate the secondary beam intensities in a projectile fragmentation separator using a doubly achromatic system [22]. Using the device parameters and settings of the magnetic spectrometer for the experiment, the transmission of the reaction products in RIBLL were simulated in the INTENSITY calculation. An estimation of the production rate after the transmission in RIBLL requires the specification of the production cross-section and the momentum distribution. The production cross-sections for the fragments in Be target were estimated using the EPAX formula [11,12]. To determine the momentum distributions of the projectile fragments in INTENSITY calculation, the statistical model of Goldhaber is used which assumes Gaussian curves for the distributions [23]. Considering a number of processes which can modify the momentum width of the fragment, the parallel and perpendicular momentum widths are calculated,

respectively, by [22]

$$\sigma_{||}^2 = \frac{(0.83p_{\rm F})^2}{5}\frac{A_{\rm f}(A_{\rm p}-A_{\rm f})}{A_{\rm p}-1} \quad (1)$$

and

$$\sigma_{\perp}^2 = \sigma_{||}^2 + \frac{A_{\rm f}(A_{\rm f}-1)}{A_{\rm p}(A_{\rm p}-1)}\sigma_2^2\,, \quad (2)$$

where $A_{\rm p}$ and $A_{\rm f}$ refer to the projectile and fragment masses, $p_{\rm F}$ is the Fermi momentum of the nucleons within the projectile, and $\sigma_2 = 195$ MeV/c is the variance of the transverse momentum at the instant of fragmentation. In INTENSITY calculation, the transmission rate for each fragment from T0 to T2 in RIBLL was obtained. According to INTENSITY calculation, the transmissions from T0 to T2 were 5–60%. Then the production yields of the fragments were derived directly after the raw counts were divided by the transmission rates. Since the scaling factor from the yield to the cross-section depends mainly on the beam intensity, the thickness and density of the target, it should be the same for each isotope. In INTENSITY calculation, the error of the ratios between the yields and the production cross-sections was less than 2.5%. So the shape of the distribution from the yields to the cross-sections would not be affected for each isotope and the experimental yields obtained in this way are comparable to the production cross-sections from fragmentation model calculation. At the same time, we have also used the method as described in ref. [19] to estimate the transmission values, in which the fragmentation model SIMON was used [24]. The results from these two methods were consistent within the estimated error bands. This conclusion indicates that the assumed momentum distributions in INTENSITY can describe the physics as in SIMON. Based on the previous experimental experience on RIBLL, the potential effect of not fully stripped fragments on the transmission values was negligible. The same conclusion was obtained in the INTENSITY calculation. The errors from this analysis are estimated to be less than 10% for fragment with 40–60% transmission, around 15% for 20–40% transmission and 35% for 5–20% transmission.

4 Discussion of the experimental results

The measured data were compared with the statistical abrasion-ablation model developed by Brohm *et al.* [7], which considers the independent nucleon-nucleon collisions in the overlap zone of the colliding nuclei and describes the collisions by a picture of interacting tubes. Assuming a binomial distribution for the absorbed projectile neutrons and protons in the interaction of a specific pair of tubes, the distributions of the total abraded neutrons and protons are determined. For an infinitesimal tube in the projectile, the transmission probabilities for neutrons (protons) at a given impact parameter b are calculated by [7]

$$t_{\rm k}(r-b) = \exp\left[-[D_{\rm n}^{\rm T}(r-b)\sigma_{\rm nk} + D_{\rm p}^{\rm T}(r-b)\sigma_{\rm pk}]\right], \quad (3)$$

where $D^{\rm T}$ is the thickness function of the target, which is normalized by $\int {\rm d}^2 r D_{\rm n}^{\rm T} = N^{\rm T}$ and $\int {\rm d}^2 r D_{\rm p}^{\rm T} = Z^{\rm T}$ with $N^{\rm T}$ and $Z^{\rm T}$ referring to the neutron and proton number in the target, respectively, the vectors r and b are defined in the plane perpendicular to beam, and $\sigma_{\rm k'k}$ is the free nucleon-nucleon cross-sections (k′, k = n for neutron and k′, k = p for proton). The thickness function of the target is given by

$$D_{\rm k}^{\rm T}(r) = \int_{-\infty}^{+\infty} {\rm d}z \rho_{\rm k}((r^2+z^2)^{1/2})\,, \quad (4)$$

with $\rho_{\rm k}$ being the neutron (proton) density distribution of the target. So the average abraded mass at a given impact parameter b is calculated by the expression

$$\langle \Delta A(b)\rangle = \int {\rm d}^2 r D_{\rm n}^{\rm P}(r)[1-t_{\rm n}(r-b)] + \int {\rm d}^2 r D_{\rm p}^{\rm P}(r)[1-t_{\rm p}(r-b)]\,. \quad (5)$$

This model is designed for the calculation of the production cross-section at relativistic energies. It is quite successful in describing the fragmentation reaction at high energies. On account of the medium effect of nucleon-nucleon collision and the larger neutron density distribution radii for exotic nuclei, two modifications were made in order to describe the nuclear collision of neutron-rich nuclei at intermediate energies [19,25]. One is the use of the in-medium nucleon-nucleon collision cross-section [26]. The other is the introduction of the separation energy dependent neutron diffuseness [27]. These modifications make this model applicable to fragmentation reaction involving neutron-rich or proton-rich nuclei over a wide energy range. It was shown that this modified model could reproduce the isotopic production cross-sections of the fragments in 44 MeV/nucleon ^{40}Ar, ^{86}Kr and ^{129}Xe induced fragmentation reactions except for the neutron-rich side of the last very heavy system [25].

The fragment production yield distributions of ^{36}Ar and ^{40}Ar are compared with the modified statistical abrasion-ablation model calculations in fig. 3 and 4. It is seen that the obtained experimental yields are compatible with the model calculations for ^{36}Ar and ^{40}Ar in some measure. The peak positions of the fragment isotopic distribution are well reproduced by the model and the agreement of the shapes of the fragment isotopic distribution between the experiment results and the calculations is also satisfactory. However, the model calculations disagree with the yields for fragments near the projectile in ^{36}Ar fragmentation. This may be partly due to the fact that the momentum distributions used in INTENSITY may deviate from the true ones at the lowest energies [22]. The degree of deviation will depend on the mass difference between the fragment and the projectile, which can cause distortions of the shapes of the isotopic distributions. For the isotopes far from the projectile, such as Li and Be, other reaction mechanisms, like, *e.g.*, multifragmentation, may contribute to their production and their yields were underestimated by the model.

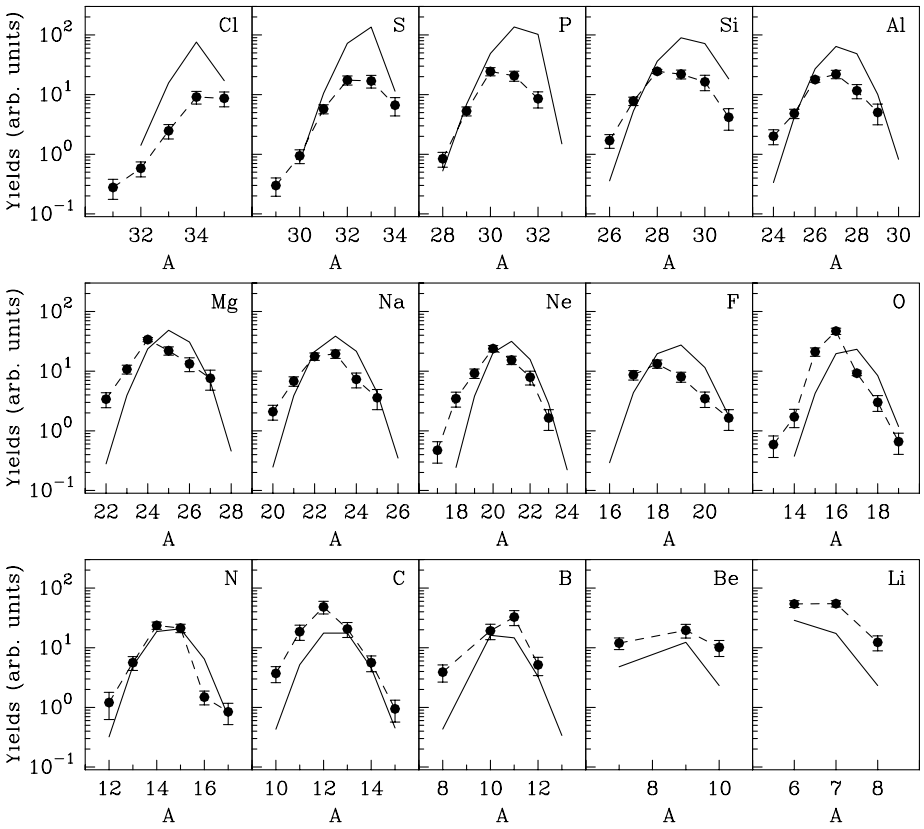

Fig. 3. Comparison of the fragment isotopic distribution produced by 69 MeV/nucleon ^{36}Ar on Be between the experimental data and the modified statistical abrasion-ablation model calculations. The solid circles are the experimental results. The solid lines are the calculations.

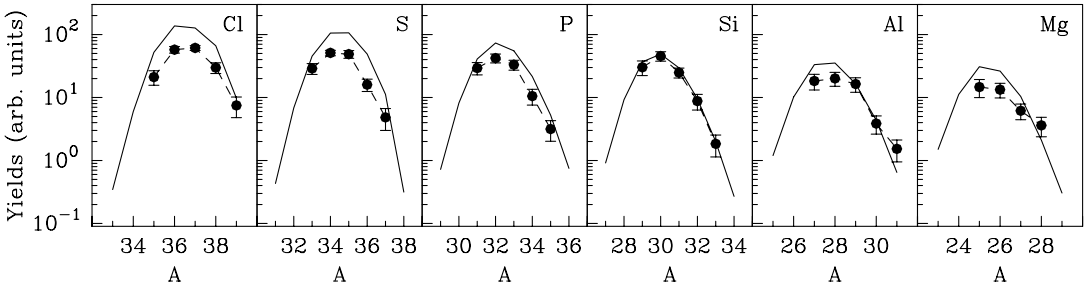

Fig. 4. Comparison of the fragment isotopic distribution produced by 55 MeV/nucleon ^{40}Ar on Be between the experimental data and the modified statistical abrasion-ablation model calculations. The solid circles are the experimental results. The solid lines are the calculations.

The isospin effect in the isotopic distributions from fragmentation of different projectiles have been investigated using the modified statistical abrasion-ablation model [19]. In this experiment the experimental data for the isospin effect can be deduced and are compared with the model calculations in fig. 5 and 6 for ^{36}Ar and ^{40}Ar. In the two figures, $A_{\rm peak}$ is the peak position of the fragment isotopic distribution extracted by a Gaussian fit to the distributions, A_β is the mass of most β-stable nucleus of the isotope determined by $Z = A_\beta/(1.98 + 0.0155 * A_\beta^{2/3})$ [12], $\Delta A_{\rm proj}$ is the mass number difference between ^{36}Ar and ^{40}Ar, and $\Delta A_{\rm peak}$ is the peak position difference of the fragmentation isotopic distribution produced by these two projectiles. Strong isospin effect arising from the different neutron excess of ^{36}Ar and ^{40}Ar is observed. With the increase of $(Z_{\rm proj} - Z)/Z_{\rm proj}$ or the violence of nuclear

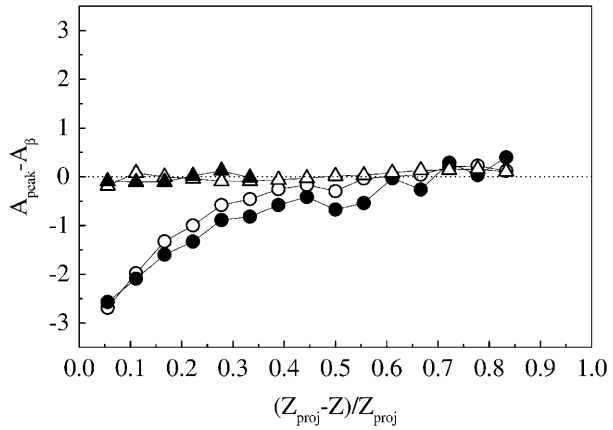

Fig. 5. The difference $A_{\rm peak} - A_\beta$ of the fragment isotopic distribution as a function of $(Z_{\rm proj} - Z)/Z_{\rm proj}$. The solid uptriangles are the experimental data of the neutron-rich projectiles ^{40}Ar. The solid circles are the experimental results of ^{36}Ar. The open uptriangles are the model calculations for ^{40}Ar. The open circles are the calculation results for ^{36}Ar.

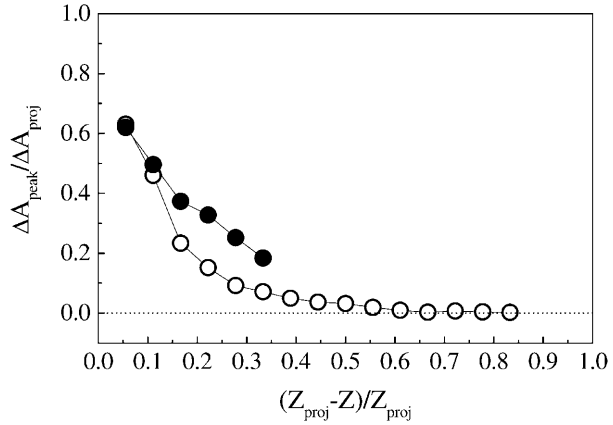

Fig. 6. The normalized peak position difference $\Delta A_{\rm peak}/\Delta A_{\rm proj}$ of the fragment isotopic distribution produced by ^{40}Ar and ^{36}Ar as a function of $(Z_{\rm proj} - Z)/Z_{\rm proj}$. The solid circles are the experimental results and the open circles are the model calculations.

reaction, disappearance of the isospin effect is seen for the experimental data, which is consistent with the model prediction [19].

5 Conclusion

In summary, the fragment isotopic distributions for 69 MeV/nucleon ^{36}Ar and 55 MeV/nucleon ^{40}Ar on a Be target were measured experimentally. After incorporating INTENSITY transmissions, the experimental yields were compatible with the modified statistical abrasion-ablation model calculations in some measure. The isotopic distributions of the fragmentation reaction products exhibited strong isospin effect for projectile ^{36}Ar and ^{40}Ar. Evidence for the disappearance of the isospin effect was found with the increase of the parameter $(Z_{\rm proj} - Z)/Z_{\rm proj}$. Since no fragment with $Z < 12$ was measured in the ^{40}Ar experiment, the complete disappearance of the isospin effect was not seen. Further experiment to measure all the fragments will help to clarify the conclusion.

This work was supported by the Major State Basic Research Development Program in China Under Contract No. G200077400.

References

1. J.D. Bowman, W.J. Swiatecki, C.F. Tang, Lawrence Berkeley Laboratory Report No. LBL- **2908**, (1973).
2. J. Hufner, K. Shafer, B. Schurmann, Phys. Rev. C **12**, 1888 (1975).
3. J. Gosset et al., Phys. Rev. C **16**, 629 (1977).
4. D.J. Morrissey et al., Phys. Rev. C **18**, 1267 (1978).
5. R. Dayras et al., Nucl. Phys. A **460**, 299 (1986).
6. A. Bonasera, M.D. Toro, C. Gregoire, Nucl. Phys. A **463**, 653 (1987).
7. T. Brohm, K.H. Schmidt, Nucl. Phys. A **569**, 821 (1994).
8. I. Tanihata et al., Phys. Rev. Lett. **55**, 2676 (1985); Phys. Lett. B **160**, 380 (1985).
9. I. Tanihata et al., Phys. Lett. B **206**, 592 (1988).
10. A. Ozawa et al., Nucl. Phys. A **673**, 411 (2000).
11. K. Summerer et al., Phys. Rev. C **42**, 2546 (1990).
12. K. Summerer, B. Blank, Phys. Rev. C **61**, 034607 (2000).
13. M.L. Miller et al., Phys. Rev. Lett. **82**, 1399 (1999).
14. J.F. Dempsey et al., Phys. Rev. C **54**, 1710 (1996).
15. B.A. Li et al., Phys. Rev. Lett. **76**, 4492 (1996).
16. B.A. Li, C.M. Ko, W. Baur, Int. J. Mod. Phys. E **7**, 147 (1998).
17. R. Pak et al., Phys. Rev. Lett. **78**, 1022 (1997); 1026
18. S. Kumar et al., Phys. Rev. C **58**, 3494 (1998).
19. D.Q. Fang et al., Phys. Rev. C **61**, 044610 (2000).
20. D.Q. Fang et al., Chin. Phys. Lett. **17**, 267 (2000).
21. J.X. Li et al., High Energy Phys. Nucl. Phys. **23**, 231 (1999) (in Chinese).
22. J.A. Winger, B.M. Sherrill, D.J. Morrissey, Nucl. Instrum. Methods B **70**, 380 (1992).
23. A.S. Goldhaber, Phys. Lett. B **53**, 306 (1974).
24. D. Durand et al., Nucl. Phys. A **541**, 266 (1992).
25. D.Q. Fang et al., High Energy Phys. Nucl. Phys. **23**, 475 (1999) (in Chinese).
26. X.Z. Cai et al., Phys. Rev., C **58**, 572 (1998).
27. J. Feng, W.Q. Shen, Y.G. Ma, Phys. Lett. B **305**, 9 (1993).